Journal of Power Sources 267 (2014) 197–202

Contents lists available at ScienceDirect

Journal of Power Sources

journal homepage: www.elsevier.com/locate/jpowsour

Short communication

Rate dependence of swelling in lithium-ion cells

Ki-Yong Oh [a], Jason B. Siegel [a], Lynn Secondo [b], Sun Ung Kim [a, b], Nassim A. Samad [a], Jiawei Qin [a], Dyche Anderson [c], Krishna Garikipati [a], Aaron Knobloch [d], Bogdan I. Epureanu [a, *], Charles W. Monroe [b], Anna Stefanopoulou [a]

[a] Department of Mechanical Engineering, University of Michigan, 2350 Hayward Street, Ann Arbor, MI 48109-2125, USA
[b] Department of Chemical Engineering, University of Michigan, 2350 Hayward Street, Ann Arbor, MI 48109-2125, USA
[c] Advanced Battery Controls R&A, Ford Motor Company, Dearborn, MI 48121, USA
[d] Photonics Laboratory, General Electric Global Research, Niskayuna, NY 12309, USA

HIGHLIGHTS

- Thermal expansion and Lithium-ion intercalation cause significant swelling.
- The swelling depends on the C-rate although the potential varies minimally.
- The phase transition in the negative electrode can be identified using ds/dQ.
- Overall shape of the swelling on the surface is constant regardless of the SOC.
- The expansion on the battery surface center is 1.5% of the entire thickness.

ARTICLE INFO

Article history:
Received 11 February 2014
Received in revised form
9 May 2014
Accepted 10 May 2014
Available online 20 May 2014

Keywords:
Lithium-ion battery
Thermal expansion
Lithiation
Strain
Swelling

ABSTRACT

Swelling of a commercial 5 Ah lithium-ion cell with a nickel/manganese/cobalt-oxide cathode is investigated as a function of the charge state and the charge/discharge rate. In combination with sensitive displacement measurements, knowledge of the electrode configuration within this prismatic cell's interior allows macroscopic deformations of the casing to be correlated to electrochemical and mechanical transformations in individual anode/separator/cathode layers. Thermal expansion and interior charge state are both found to cause significant swelling. At low rates, where thermal expansion is negligible, the electrode sandwich dilates by as much as 1.5% as the charge state swings from 0% to 100% because of lithium-ion intercalation. At high rates a comparably large residual swelling was observed at the end of discharge. Thermal expansion caused by joule heating at high discharge rate results in battery swelling. The changes in displacement with respect to capacity at low rate correlate well with the potential changes known to accompany phase transitions in the electrode materials. Although the potential response changes minimally with the C-rate, the extent of swelling varies significantly, suggesting that measurements of swelling may provide a sensitive gauge for characterizing dynamic operating states.

1. Introduction

Automobile manufactures have recently accelerated battery development efforts to meet stringent fuel economy and emission standards for future hybrid electric vehicles (HEVs) and electric vehicles (EVs), with most research focused on the design of lithium-ion (Li-ion) battery packs [1,2]. Cycle life is a particular concern because of the high cost of the battery pack relative to that of the total vehicle. The mechanical response of battery cells during cycling impacts cycle life since fatigue may lead to capacity loss and eventual failure [3]. To date little is understood about the effects of stress and strain on cell-level performance, because data evaluating coupled electrochemical and mechanical phenomena is sparse. However, it becomes more and more significant to understand the stress and strain characteristics of Li-ion battery cells. This understanding would help develop strategies to reduce cell-level volume changes, which could ideally prolong cycle life by reducing the tendencies of cell materials to mechanically degrade.

Many efforts have been devoted to measuring periodic swelling of electrode materials in Li-ion batteries under charge and

* Corresponding author. Tel.: +1 734 647 6391; fax: +1 734 615 6647.
E-mail address: epureanu@umich.edu (B.I. Epureanu).

http://dx.doi.org/10.1016/j.jpowsour.2014.05.039
0378-7753/

discharge conditions [4–8]. As a consequence of swelling, large periodic stresses – potential internal fatigue loads – can be experienced by cells stacked and constrained in a battery pack. The data presented here shows that the volume change of Li-ion battery cells is far from insignificant. Large periodic loads and dynamic expansion should be taken into consideration during battery pack modeling and design.

Information is available about mechanical effects from a microscopic perspective. Research into the stresses generated within active materials and the porous electrodes that support them has been carried out [9–11]. The dependency of capacity fade on initial stack pressure has also been examined [12]. These studies provide a useful foundation for understanding the physical phenomena within active materials associated with Li-ion intercalation and deintercalation. But the relationships among mechanical forces remain poorly understood, making it difficult to predict how overall expansion or contraction of the electrode sandwich arises from stresses and strains within its constituent elements. Moreover, the behavior of active materials during high-rate operation, where local joule heating and changes in charge state may both cause deformation, has not been investigated in great detail.

A high-precision displacement sensor was used to quantify the volume changes arising from Li-ion intercalation in an unconstrained graphite/nickel–manganese–cobalt-oxide (NMC) battery cell, whose temperature was regulated in a thermal chamber. Swelling of the cell was studied as a function of the state-of-charge (SOC) and the charge/discharge rate (C-rate). The extent of swelling was found to vary significantly with both experimental control parameters. When the rate was sufficiently low to main a relatively constant cell temperature, swelling in the fully charged state was generally as high as 1.5% relative to a cell equilibrated at 0% SOC. By examining the derivative of swelling with respect to capacity, different phase transitions within the electrode materials can be identified. These correlate to the sudden changes in open-circuit potential that occur with the phase changes in electrode materials [13].

The extent of swelling was also found to exhibit strong rate dependence, despite the fact that cell potential vs SOC did not change significantly over the range of C-rates investigated. Thus information about swelling may provide a more sensitive gauge of a battery cell's dynamic state than its voltage.

2. Experimental

A flat-wound type prismatic (120 mm × 85 mm × 13.5 mm width × height × depth) 5 Ah Li-ion battery cell was obtained from a Ford Fusion HEV battery pack. Dissection of a similar cell from the same pack showed that the cell interior contains a single flat-wound electrode jellyroll that fits snugly within the battery casing; thus, through the depth dimension z, the cell interior comprises 52 stacked, essentially planar sandwich layers, each of which lies predominantly in the x–y plane labeled in Fig. 1.

The cell casing, the thickness of the positive electrode plate, the negative electrode plate were measured with calipers (650 μm, 80 μm, 80 μm respectively). The separator is 25 μm in general [14]. Thus, each anode/separator/cathode layer (consisting of 1 positive/negative electrode plate and 2 separators) has a thickness of 210 μm and the estimated total thickness of the jellyroll is 11.0 mm considering the number of stacks (52). The estimated total thickness of the jellyroll corresponds well with the measured depth of the casing (12.2 mm) considering additional insulation materials, which is formed on the outer circumference of a jellyroll to secure electrical insulation between the jellyroll and the cell casing.

When unrolled, the sandwich consists of an aluminum positive current collector coated on both sides with the lithium nickel/manganese/cobalt oxide (NMC) material, a microporous polyethylene separator material, and a copper negative current collector coated on both sides with a graphite intercalation material (Li_xC_6) [16].

High-precision contact-type displacement sensors with 1 μm accuracy and 0.1 μm resolution (Keyence GT2-H12KL, Japan) were used for displacement measurements. A low-stress type head with contact force of under 0.3 N was used to minimize the contact force exerted on the battery's surface by the sensor head.

A fixture was made from ABS plastic using a rapid-prototyping machine (Dimension Elite FDM, USA). In the fixture, the prismatic battery cell was constrained at its eight corners with ABS plastic set-screws, but was otherwise unconstrained for free swelling condition. The fixture was designed to minimize the contact area between the set-screws and the battery, which was less than 0.4 cm^2 total. Note also that the modulus of elasticity for the fixture material (ABS plastic) is 2.2 GPa, which is more than 30 times smaller than that for aluminum (68 GPa). Thus, the limitations that the fixture placed on the free swelling of the cell were determined to be negligible.

The fixture was placed inside a thermal chamber (ESPEC BTZ-133, Japan) that maintained a constant ambient temperature of 25.5 °C for all tests. Three thermocouples were also placed on the cell exterior to measure surface temperatures in two locations, as well as the near-surface air temperature. One thermocouple was installed on the center of the battery cell (in a location that avoided interference with a displacement sensor). Another thermocouple was installed on the top of the battery between the positive and the negative terminals. The third thermocouple was installed between the fixture and the battery cell to measure near-surface ambient temperature.

The Li-ion intercalation/deintercalation into the electrode occurs mainly in a direction perpendicular to the electrodes during

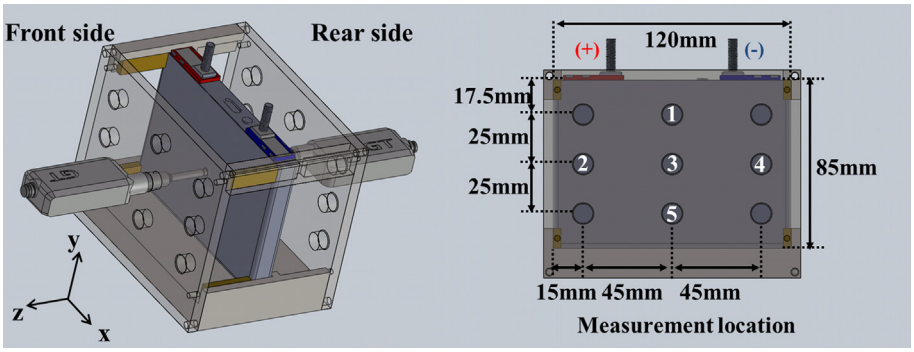

Fig. 1. Schematic diagram of the experimental setup showing the fixture, the cell, and the sensor locations 1–5.

charge and discharge. Therefore, swelling in the z direction was measured, which is perpendicular to the electrodes (as reported in Ref. [16], and also verified by dissection of a cell in an Ar glovebox). The configuration of sensors within the fixture is shown in Fig. 1. Note that it was observed that no gap existed between the flat-wound jellyroll and the casing in the z direction. In contrast, there were observed to be gaps between the casing and the jellyroll on the sides and the top of the cell. Hence, swelling in the transverse directions was determined to be negligible and was not measured.

In a first experiment the relative expansion in the z direction was measured at five locations labeled 1–5 in Fig. 1, to assess the uniformity of the swelling distribution in the plane of the multi-layer electrode sandwich. For each experiment the battery was charged using a standard constant-current, constant-voltage charging profile at 2 A; the voltage was clamped after reaching 4.1 V, at which it was held until the current tapered to C/100 (50 mA). The battery then was allowed to rest at open circuit for 3 h to ensure thermal equilibrium prior to discharging. This experiment was performed using a 0.4C discharge rate to mitigate the effects of swelling due to thermal expansion.

In a second experiment, opposing displacement sensors were placed at the geometric centers on both faces of the cell normal to z (location 3 shown in Fig. 1). The net displacement was measured with respect to the charge state during discharge at a variety of C-rates using a standard constant-current, constant-voltage charging/discharging profile. All discharges were performed at fixed C-rate down to 2.5 V. Measurements with exterior thermocouples showed that the lowest current used, 0.4C (2 A), did not cause significant heating; this was confirmed by the observation that the battery-cell surface remained within 0.5 °C of the 25.5 °C ambient temperature throughout the discharge process. Data at 0.4C therefore allow direct correlations to be made between swelling and Li-ion intercalation in a cell sandwich, without significant convolution with thermal expansion. In contrast, the cell surface temperature deviated more significantly from the ambient at higher rates – as much as 3 °C higher in the 5.0C case.

3. Results and discussion

Fig. 2 illustrates the expansion measured at five locations on the front surface, and at the center location on the rear surface, during a 0.4C charge/discharge. The geometric centers on the x–y surfaces of the battery travel outward by 99.8 μm and 103.2 μm, respectively after charge; both return to their original positions at the end of discharge. Given that the thickness of the discharged battery is 13.5 mm, the total normal strain in the z direction in the center of the cell amounts to 1.5%. It can be inferred that swelling of active materials is translated into swelling of the case. On an average basis, the dilation of each anode/separator/cathode layer would also be expected to match this 1.5%. Because the amount of swelling is not small, expansion should be considered in the design of the battery pack to improve the reliability and predict the lifespan as periodic stress is generated, not only within the electrode sandwich or a single cell, but also within the battery pack.

In general, graphite anode materials exhibit 10% volume expansion under charge [17], and irrecoverable volume increase at a graphite intercalation material due to solid-electrolyte interphase formation is at least 4% of initial thickness [18]. Therefore 6% of reversible swelling from a graphite intercalation material is able to be translated into 2% expansion of total thickness, in that the negative-electrode volume occupies about 30% of the jellyroll volume (taking the thickness of Cu foil to be 10 μm [16]). In contrast, the volume contraction from a nickel/manganese/cobalt-oxide positive electrode is less than 1% [19]. So 1% of contraction from

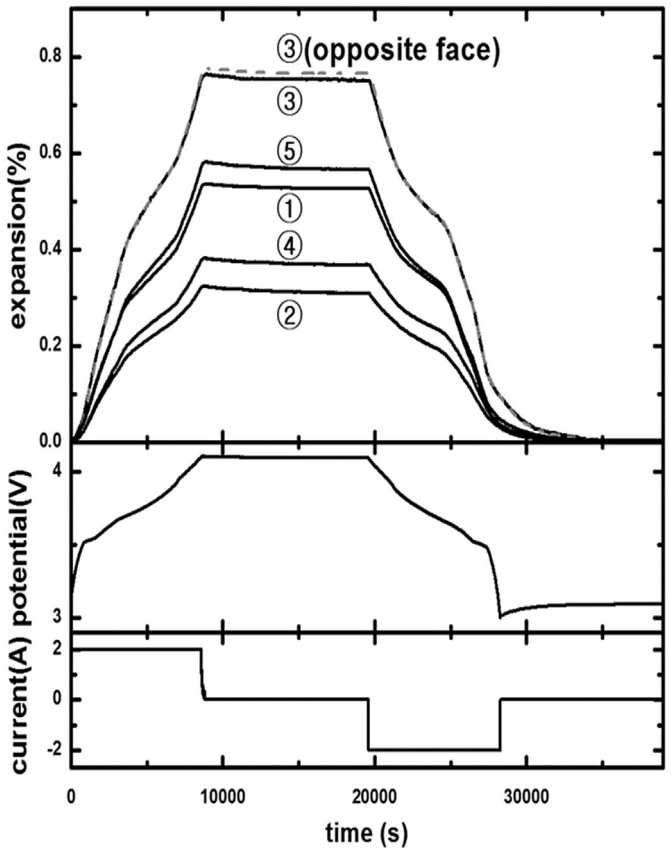

Fig. 2. Expansion (swelling) trends over time; encircled digits indicate measurement points shown in Fig. 1; the measured current and potential over time are shown in the bottom plots.

the cathode material can be translated into ~0.5% contraction of the total thickness, as the cathode volume also occupies about 30% of the jellyroll. In consideration of the volume expansion of the negative electrode and the volume contraction of the positive electrode, total variation of the volume is 1.5%, which is well matched with experimental result. It is also found that the overall shape of the measured swelling is similar to the average interlayer spacing of graphite within the negative electrode [20]. These results corroborate the hypothesis that the SOC-dependent exterior volume change can be mainly attributed to changes within the negative electrode.

As expected, displacements in the geometric centers of the battery faces are the largest; displacements reduce near the edges of the cell because of mechanical constraints imposed by the battery casing. The smallest expansion was measured at locations 2 and 4. Note also that dissection of the cell showed that the current collectors flank the flat-wound jellyroll on its left and right edges (approximately beneath the positive and negative exterior terminals) [16]; since they undergo no chemical transformation they would not be expected to dilate with changing SOC at fixed temperature. Hence, the empty space along the left and right edges of the current collectors (where no internal force due to the lithium-ion intercalation is exerted on the casing) leads to the smallest expansion observed at locations 2 and 4. Moreover, the relatively large thickness of the casing and the higher modulus of elasticity of the aluminum casing (much larger than that of the electrode and the separator) might result in location dependency of the swelling [15,21].

Most significantly, the cell was found to expand asymmetrically, with a statistically significant difference upon completion of

charging. The bottom (location 5) swells more than the top (location 1); the swelling of the top and the bottom side are 72.4 μm and 78.8 μm respectively. This is due to the different thickness of the top and the bottom of the casing; the thicknesses of the top and the bottom are 1500 μm and 650 μm respectively. Thus, the stiffness of the top of the casing is much higher than that of the bottom, and hence the bottom side of the casing is easier to deform than the top. It might also result in the empty space between the top of the case and the jellyroll because no internal force due to the lithium-ion intercalation is exerted on the empty space of the casing. The asymmetry between left/right sides can be due to differing material properties and complex shapes of both current collectors and clamps, which fix different positions of the jellyroll at each current collector.

The surface temperature of the battery remains within a range smaller than 0.5 °C during charge and discharge at the rate of 0.4C. Thus, the effects of thermal gradients on the swelling shape of the battery in the x–y plane are likely negligible at 0.4C. In contrast, these thermal gradients may affect the shape of the swelling of the cell in the x–y plane at high C-rates because the internal heating of the electrodes creates a thermal gradient.

The overall strain distribution appears to remain the same during charging and discharging. Fig. 3(a) and (b) illustrates the variation of expansion with respect to SOC. The ratio of expansion between center and other locations (L_{Avg}, R_{Avg}, T_{Avg}, B_{Avg}) is constant throughout the range of SOC. This could suggest that the reaction distribution throughout the jellyroll is relatively constant. Regardless, the constant shape of the surface-strain distribution suggests that a single point measurement can be used to accurately quantify the entire cell swelling at the C-rates studied.

Fig. 4 shows the swelling, cell potential, and measured surface temperature at the center of the battery case surface during discharges at a variety of C-rates.

The residual swelling at end-of-discharge was found to depend strongly on discharge rate, despite the fact that cell potentials did not change significantly. Although the amount of charge processed at all C-rates was nearly identical, at higher rates the battery had not returned to its initial thickness when the voltage reached 2.5 V. The higher C-rate operation leads to the larger temperature increase, as shown at the bottom of Fig. 4. The total thermal swelling of the cell results from thermal swelling of each cell component. However, it is hard to estimate the thermal swelling of each cell component based on measured cell-level thermal swelling. When a jellyroll is fabricated, positive/negative electrodes are wound and the resulting jellyroll is clamped and welded to the buss bars at each side [16]. This manufacturing process results in pre-stress and possibly plastic deformation of layers inside the jellyroll. Thus, to estimate the impact of each component on the thermal swelling, the pre-stress and the modulus of elasticity of each component should be characterized also. However, the estimation of the pre-stress in the jellyroll is difficult without exact information regarding the manufacturing process. Moreover, the modulus of elasticity of each component was not available. Hence, the contribution of each cell component is hard to estimate given only cell-level thermal expansion data. However, equivalent mechanical properties of the cell (such as equivalent modulus of elasticity and equivalent coefficient of thermal expansion) can be used to create

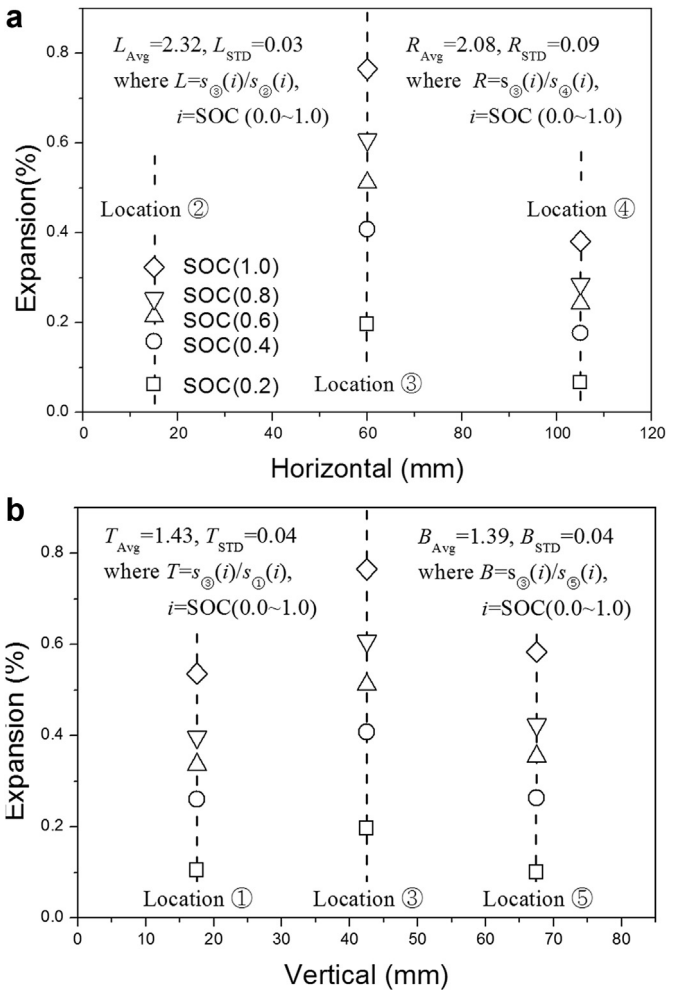

Fig. 3. The spatial distribution of swelling; subscripts Avg and Std indicate average values and standard deviation levels; each dashed line indicates a measurement location.

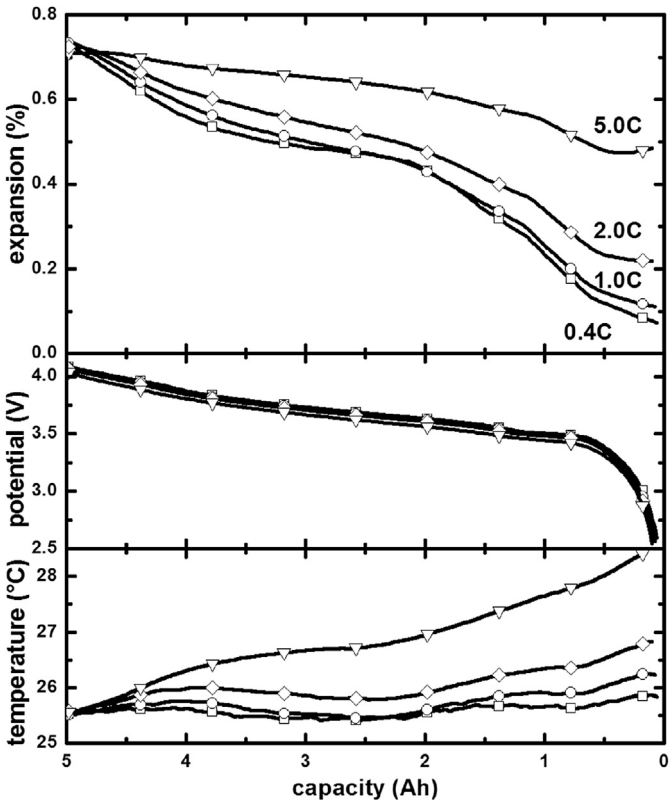

Fig. 4. Expansion, potential, and surface temperature versus capacity for discharge at a variety of C-rates on the center of the surface of the battery (location 3 in Fig. 1).

accurate battery swelling models for efficient control and health management.

Fig. 5 illustrates the response during the open-circuit rest period after discharge, during which the swelling continued to decrease and finally returned its initial value. The measured data reveal a relaxation with two time constants in the swelling, namely

$$s = a_0 + a_1 e^{-t/\tau_1} + a_2 e^{-t/\tau_2}, \quad (1)$$

where s is the swelling measured at location 3 (Fig. 1). The coefficients a_0, a_1, and a_2, and the time constants τ_1 and τ_2 are obtained by curve fitting the measured relaxation data. The faster response can be attributed to thermal relaxation, because its time constant is consistent with the one extracted from measured surface temperature, shown in the lower subplot of Fig. 4. The slower response may be caused by visco-elastic mechanical relaxation. A small increase of swelling is observed at the beginning of the relaxation period for 5C discharge, which correlates with the continued rise in surface temperature following the cessation of the current.

These experiments were carried out in the thermal chamber, which regulates ambient temperature to 25.5 °C. The temperature of the cell converges to ambient temperature, as shown in the bottom of Fig. 5. The temperature was continuously controlled during charge and discharge. Thus, the internal heat (e.g., produced from joule heat and entropy heat) is removed from the chamber during operation, and so the ambient temperature does not increase. Hence, the thermal swelling (at constant ambient temperature) is smaller than the thermal swelling in an insulated/adiabatic environment (where the temperature increases). In conclusion, the thermal swelling depends on the C-rate and the heat dissipation rate. Also, the heat dissipation from the cells is important for the design of battery packs (to mitigate the thermal swelling and thermal stress).

The role of individual electrodes in the overall swelling process can be understood by analyzing the derivative of swelling s with respect to capacity Q, namely ds/dQ. The swelling derivative is compared with the derivative of potential with respect to capacity,

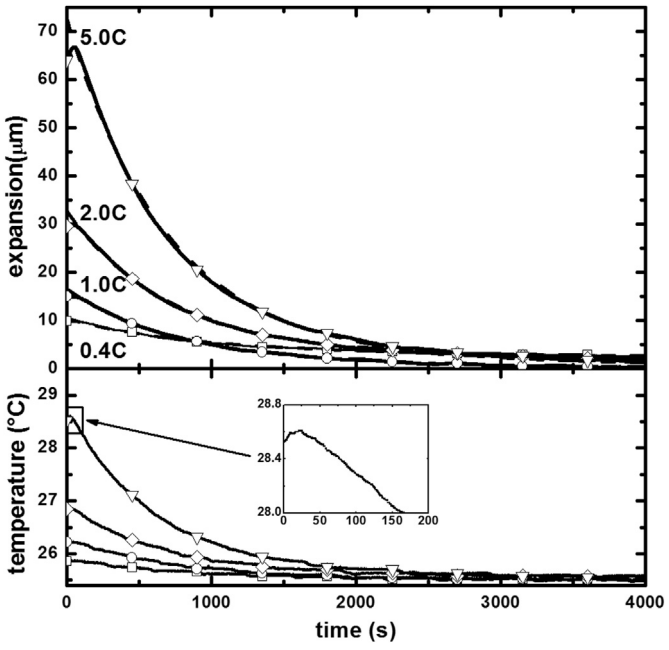

Fig. 5. Relaxation and surface temperature at the end of the discharge at a variety of C-rates on the center of the surface of the battery (location 3 in Fig. 1).

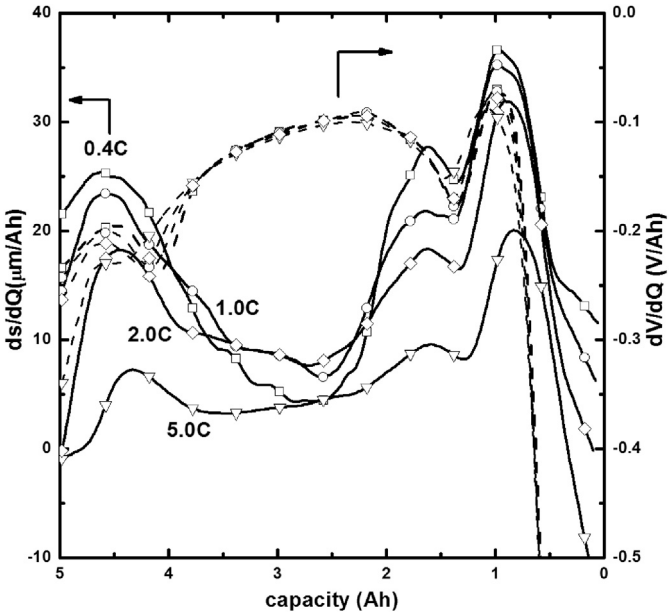

Fig. 6. ds/dQ and dV/dQ at a variety of C-rates on the center of the surface of the battery for discharge (location 3 in Fig. 1).

dV/dQ, in Fig. 6. The lines denote ds/dQ curves and the dot lines denote dV/dQ curves in Fig. 6. Most of the local maxima of dV/dQ correspond to phase transitions known to occur in graphite negative electrodes; the voltages at which these maxima occur are similar to previously reported results [13,22]. Phase transitions of the positive NMC electrode do not appear to have strong signatures, because the NMC structure does not fill in stages the way the graphite lattice does, and undergoes smaller volume changes [8,23]. Therefore the macroscopic swelling at low rates appears to be dominated by the negative electrode, which corresponds well with calculated volume change of the positive and negative electrode.

The peak locations for ds/dQ and dV/dQ differ slightly at different C-rates, suggesting that higher discharge rates correlate with later signatures of phase transition. This could owe to the fact that multiple co-existing phases exist in the negative electrode, which may be present to different extents when the surface overpotential in the electrode is higher [24]. The peak shift may also owe to lagging thermal expansion, as shown during the relaxations at 5C in Fig. 6. It is also possible that the lag owes to delay of structural change due to slow diffusion of Li-ion [25] or a visco-elastic effect, whereby the stresses induced by lithium intercalation/deintercalation take some time to manifest as macroscopic strain. The ds/dQ might be applicable for fault diagnosis, prognosis and estimation of aging of the battery cell in that the swelling of the battery cell is sensitive factors affecting cell performance.

4. Conclusions

The surface swelling of a 5 Ah Li-ion battery cell with a NMC cathode was studied at various C-rates. Significant strain was measured at the geometric center of the battery case: the anode/separator/cathode layers appear to dilate in thickness by 1.5% as the cell is taken from 0% to 100% SOC. The contraction observed on discharge was found to depend strongly on the C-rate, although the potential varied minimally. Thermal and mechanical relaxations appeared to contribute to the strain response at high discharge rates. Signatures of phase transitions in the negative electrode could be identified by analyzing strain as a function of capacity; this

response was also found to depend strongly on the C-rate. The overall distribution of strain across the battery surface retained the same shape regardless of SOC, suggesting that the current distribution within the electrode jellyroll is relatively uniform.

Disclaimer

Acknowledgments

The information, data, or work presented herein was funded in part by the Advanced Research Projects Agency-Energy (ARPA-E), U.S. Department of Energy, under Award Number DE-AR0000269.

References

[1] T.M. Bandhauer, S. Garimella, T.F. Fuller, J. Electrochem. Soc. 158 (3) (2011) R1–R25.
[2] X. Hu, S. Lin, S. Stanton, W. Lian, IEEE Trans. Industry Appl. 47 (4) (2011) 1692–1699.
[3] J. Shim, R. Kostecki, T. Richardson, X. Song, K.A. Striebel, J. Power Sources 112 (2002) 222–230.
[4] J.B. Siegel, A.G. Stefanopoulou, P. Hagans, Y. Ding, D. Gorsich, J. Electrochem. Soc. 160 (8) (2013) A1031–A1038.
[5] X. Wang, Y. Sone, G. Segami, H. Naito, C. Yamada, K. Kibe, J. Electrochem. Soc. 154 (1) (2007) A14–A21.
[6] N. Zhang, H. Tang, J. Power Sources 218 (2012) 52–55.
[7] D. Liu, Y. Wang, Y. Xie, L. He, J. Chen, K. Wu, R. Xu, Y. Gao, J. Power Sources 232 (2013) 29–33.
[8] F. Kaasik, T. Tamm, M.M. Hantel, E. Perre, A. Aabloo, E. Lust, M.Z. Bazant, V. Presser, Electrochem. Commun. 34 (2013) 196–199.
[9] J. Christensen, J. Electrochem. Soc. 157 (2010) A366–A380.
[10] J. Christensen, J. Newman, J. Solid State Electrochem. 10 (5) (2006) 293–319.
[11] J. Christensen, J. Newman, J. Electrochem. Soc. 153 (2006) A1019–A1030.
[12] J. Cannarella, C.B. Arnold, J. Power Sources 245 (2014) 745–751.
[13] I. Bloom, A.N. Jansen, D.P. Abraham, J. Knuth, S.A. Jones, V.S. Battaglia, G.L. Henriksen, J. Power Sources 139 (2005) 295–303.
[14] D. Shi, X. Xiao, X. Huang, H. Kiaa, J. Power Sources 196 (2011) 8129–8139.
[15] A. Sheidaei, X. Xiao, X. Huang, J. Hitt, J. Power Sources 196 (2011) 8728–8734.
[16] K. Nansaka, Y. Yamauchi, United States Patent US 8216715 B2, 2012.
[17] T. Ohzuku, Y. Iwakoshi, K. Sawai, J. Electrochem. Soc. 140 (9) (1993) 2490–2498.
[18] J.H. Lee, H.M. Lee, S. Ahn, J. Power Sources 119–121 (2003) 833–837.
[19] Y. Koyama, I. Tanaka, H. Adachi, Y. Makimura, T. Ohzuku, J. Power Sources 119-121 (2003) 644–648.
[20] R. Yazami, Y. Reynier, J. Power Sources 153 (2006) 312–318.
[21] Y. Kim, J.B. Siegel, A.G. Stefanopoulou, in: 2013 American Control Conference. Washington, USA, 2013.
[22] H.M. Dahn, A.J. Smith, J.C. Burns, D.A. Stevens, J.R. Dahn, J. Electrochem. Soc. 159 (2012) A1405–A1409.
[23] I. Bloom, L.K. Walker, J.K. Basco, D.P. Abraham, J.P. Christophersen, C.D. Ho, J. Power Sources 195 (2010) 877–882.
[24] K.G. Gallagher, D.W. Dees, A.N. Jansen, D.P. Abraham, S.H. Kang, J. Electrochem. Soc. 159 (2012) A2029–A2037.
[25] X. Wang, Y. Sone, S. Kuwajima, J. Electrochem. Soc. 151 (2) (2004) A273–A280.